Analysis of time-resolved scattering from macroscale bacterial colonies

Euiwon Bae
Purdue University
School of Mechanical Engineering
West Lafayette, Indiana 47906

Padmapriya P. Banada
Karleigh Huff
Arun K. Bhunia
Purdue University
Department of Food Science
Molecular Food Microbiology Laboratory
West Lafayette, Indiana 47906

J. Paul Robinson
Purdue University
Bindley Bioscience Center
Purdue University Cytometry Laboratories
Department of Basic Medical Sciences
School of Veterinary Medicine
and
Weldon School of Biomedical Engineering
West Lafayette, Indiana 47906

E. Daniel Hirleman
Purdue University
School of Mechanical Engineering
West Lafayette, Indiana 47906

Abstract. We investigate the relationship of incubation time and forward-scattering signature for bacterial colonies grown on solid nutrient surfaces. The aim of this research is to understand the colony growth characteristics and the corresponding evolution of the scattering patterns for a variety of pathogenic bacteria relevant to food safety. In particular, we characterized time-varying macroscopic and microscopic morphological properties of the growing colonies and modeled their optical properties in terms of two-dimensional (2-D) amplitude and phase modulation distributions. These distributions, in turn, serve as input to scalar diffraction theory, which is, in turn, used to predict forward-scattering signatures. For the present work, three different species of *Listeria* were considered: *Listeria innocua*, *Listeria ivanovii*, and *Listeria monocytogenes*. The baseline experiments involved the growth of cultures on brain heart infusion (BHI) agar and the capture of scatter images every 6 h over a total incubation period of 42 h. The micro- and macroscopic morphologies of the colonies were studied by phase contrast microscopy. Growth curves, represented by colony diameter as a function of time, were compared with the measured time-evolution of the scattering signatures. [DOI: 10.1117/1.2830655]

Keywords: scattering; biomedical optics detection; diffraction; imaging.

Paper 06332RR received Nov. 14, 2006; revised manuscript received Aug. 28, 2007; accepted for publication Oct. 26, 2007; published online Jan. 16, 2008. This paper is a revision of a paper presented at the SPIE conference on Optics for Natural Resources, Agriculture, and Foods, Oct. 2006, Boston, Mass. The paper presented there appears (unrefereed) in SPIE Proceedings Vol. 6381.

1 Introduction

The ability to rapidly identify and classify food-borne pathogens is important to the food industry as well as public safety.[1,2] There are various methods for identifying bacteria, including morphological methods, serological methods, proteomics, and genomics. Among these approaches, morphological differences can be exploited if the interrogating agents such as photons are capable of sensing the variation of the micro/macroscopic differences among different species. Optical diagnostics have been widely applied to characterizing and sensing in engineering production and biological fields.[3,4] In the biophotonics area, most of the traditional identification techniques rely on either immunoassay (antibody-antigen reaction) or on spectroscopic methods such as fluorescence.[5,6] These specialized techniques to create differentiation show high specificity, but at the same time require considerable presample preparation or treatment. Alternatively, methods based on elastic light scattering potentially have considerable advantage, since less sample preparation would be required. Some studies exploiting elastic scattering have been published[7–9] and show significant differences in scattering signature among different species that could be used to identify and classify the types of bacteria. These studies,[7–9] however, were focused on testing bacteria in a liquid suspension, either as single bacterial cells or as ensembles. The former face signal-to-noise limitation in practical application, while the latter require some averaging technique in physical modeling.

Here we take a different approach that leverages a substantial body of standard laboratory protocol. It starts with individual bacteria, plated on a medium, that divides and can eventually grow into a millimeter-size colony. In the work reported here, we interrogate the colonies with a laser beam of approximately the same diameter as the colony. The laser beam is directed normal to the surface of the growth medium, and the forward-scattered laser light is analyzed. This label-free and agent-free bacterial colony detection method was recently proposed from different points of view. Guo[10] and Banada et al.[11] showed that a forward scatterometer is an effective tool to rapidly differentiate the types of bacteria species, such as *E. coli*, *Salmonella enterica*, and *Listeria* species. Bayraktar et al.[12] presented a feature extraction model using Zernike moments to efficiently identify and classify the bacterial species from their respective scatterograms. Bae et al.[13] provided a biophysical modeling of the scatterograms from three types of *Listeria* species by modeling the bacterial colony as an amplitude/phase modulator.

Address all correspondence to Euiwon Bae, School of Mechanical Engineering, Purdue University, 585 Purdue Mall, West Lafayette, Indiana 47906; Tel: 765–494–4762; Fax: 765–494–0539; E-mail: ebae@purdue.edu

1083-3668/2008/13(1)/014010/8/$25.00 © 2008 SPIE

The scattering patterns we observe are closely related to the state of growth, along the characteristic sigmoid curve, of the bacterial colony. Since colonies of different species and strains grow at different rates at different stages of their existence, it is beneficial to investigate the relationship of growth time and scattering pattern. In this work, we performed time-resolved experiments to reveal a correlation between scattering pattern, colony growth time, and the microscopic and macroscopic physical properties of the bacterial colony. Three closely related *Listeria* species, *L. innocua*, *L. ivanovii*, and *L. monocytogenes*, were selected for the study. *Listeria monocytogenes* is a food-borne human pathogen with 20% mortality among immunocompromised people. *L. innocua* is a non-pathogenic species, while *L. ivanovii* is pathogenic to animals. To enable these experiments, and also to develop a prototype for future diagnostic applications, we redesigned the forward-scattering platform and named it bacteria rapid detection using optical scattering technology (BARDOT).[13]

Section 2 describes the experimental setups, sample preparation, and types of parameter that are measured. Section 3 describes the time-dependent scattering measurement and its correlated parameters. Last, Section 4 shows the new findings and understanding of bacterial colony scattering.

2 Materials and Methods

2.1 *System Description*

The forward scatterometer consists of a laser source, a sample holder, and an imaging screen. As shown in Fig. 1(a), the first version of our instrument[10,11] used a 635-nm diode laser as the light source and a low-resolution digital camera to acquire images. This device revealed the overall characteristics of the scattering patterns but at a lower resolution than is needed. The system was redesigned and constructed as BARDOT,[13] shown in Fig. 1(b). The new system is equipped with a laser diode module of 635-nm wavelength, an XY stage to move the sample, and a 640×480 pixel monochromatic IEEE-1394 CCD image sensor to acquire the scattering images. The new system uses a motor-controlled stage system, which reduced the total time of scattering measurement. The sample holder platform was also attached and can hold samples 2 to 4 in. in diameter, which are the typical size of a Petri dish. The design decision for a monochromatic CCD image sensor was taken to maximize the quantum efficiency, and the 7.4-μm-unit pixel size provided higher-resolution images. This new research system also enabled interrogation of near-field and far-field scattering characteristics to facilitate developing accurate physics-based models for the light scattering phenomena.

2.2 *Sample Preparation and Method*

When bacterial cells are incubated on an agar plate, their growth rate and pattern is the well-known sigmoid curve, which shows three phases: lag, exponential, and stationary. Since we are measuring the scattering response from bacterial colonies, it is critical to identify the relationship of colony growth with scattering pattern. *Listeria innocua*, *Listeria monocytogenes*, and *Listeria ivanovii* cultures were selected for our experiments. Each bacterium was grown in brain heart infusion (BHI) broth at 37°C for 15 to 18 h. Respective dilutions are plated on the surface of BHI agar so as to obtain 30 to 50 colonies per plate and are incubated at 37°C. Each

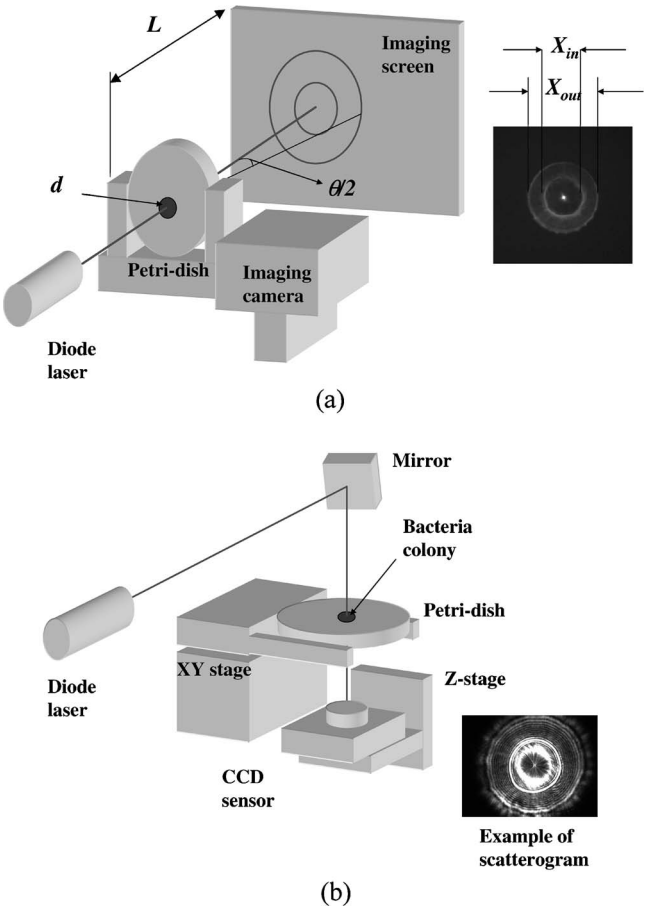

Fig. 1 Schematic diagram and parameter definition for (a) forward scatterometer and (b) BARDOT platform. L is the distance from bacterial colony to screen, d is the diameter of the colony, $\theta/2$ is the half-scattering angle, X_{out} and X_{in} are the diameters of the largest ring and the bright ring at the center.

species is cultured on six separate BHI agar plates, with half started incubating at zero h, while the other half is started 6 h later. Each bacterial colony is numbered, and every 6 h, three measurements are performed on one of the plates, with 10 to 15 colonies per plate. The three measurements are the forward scatterometer, BARDOT scattering, and phase contrast microscope images. The forward scatterometer and BARDOT systems reveal complementary scattering characteristics of the colony. The scatterogram from the forward scatterometer is displayed on the screen while the camera captures the image, and the diameters of X_{in} and X_{out} are measured using a ruler. For BARDOT, the image is captured using the CCD sensor directly. The phase contrast microscope (LEICA, Model DMLB, Wetzlar, Germany) image is recorded to provide colony diameter and two dimensional (2-D) phase information. The colony diameter is recorded by applying a built-in calibrated measurement function for a $10\times$ objective in the phase contrast microscope. The data from the microscope is used to develop a physical model for the colony morphology that is, in turn, used to inform the modeling of the physics of the scattering pattern formation.

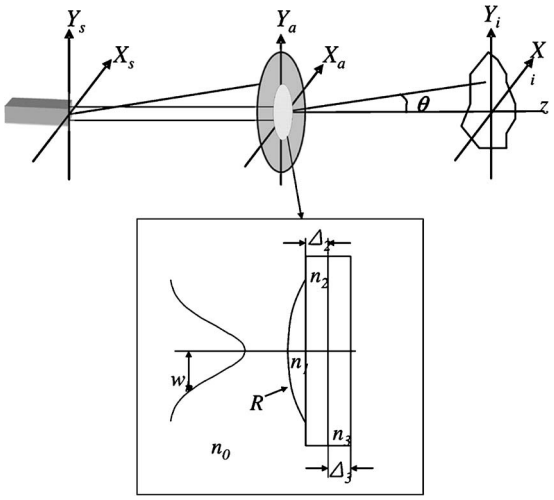

Fig. 2 Definition of coordinate system and model parameters for the bacterial colony scattering. X_s, Y_s, X_a, Y_a, and X_i, Y_i denote the source, aperture, and imaging coordinate system. Inset: w denotes the radius of the incident beam; R is the curvature of the colony surface; n_1, n_2, n_3 are the refractive indices for the colony, agar, and Petri dish; Δ_2 and Δ_3 are the thickness of the agar and Petri dish.

2.3 *Modeling Scattering Response*

The three-dimensional (3-D) vector nature of light propagation can be simplified as 2-D when the dimensions of the diffracting object are larger than the wavelength and the diffracted light is measured far away from the object.[14,15] In addition, when there is a series of amplitude/phase modulation elements such as diffraction gratings or lenses between the object and the imaging plane, the amplitude/phase modulation is mathematically formulated as a kernel in the diffraction equation. These effects are utilized in optical vortices[16] and spatial light modulators,[17] observed in telescopic optics,[18] and analyzed as spatial phase modulation (SPM) in characterizing liquid crystal material.[19–21]

We define coordinate systems for source, bacterial colony, and image plane as X_s, Y_s; X_a, Y_a; and X_i, Y_i, respectively, as shown in Fig. 2. Assuming a TEM_{00} mode of laser beam centered on the z axis with its waist on the $z=0$ location, the electric field on the source plane can be expressed as:

$$E(x_s,y_s,z) = E_0\left\{\frac{w_0}{w(z)}\exp\left[-\frac{(x_s^2+y_s^2)}{w^2(z)}\right]\right\} \times\exp\left\{i\left[kz-\tan^{-1}\left(\frac{z}{z_0}\right)\right]\right\} \times\left\{\exp\left[ik\frac{x_s^2+y_s^2}{2R(z)}\right]\right\}, \quad (1)$$

where x_s, y_s are the points on the source plane, k is the wave vector, and E_0 is the on-axis field strength. The three bracketed terms account for variations of amplitude of field, longitudinal phase, and radial phase, respectively. The variation of beam waist $w(z)$ and radii of the wavefront $R(z)$ is expressed as:[15]

$$w^2(z) = w_0^2\left[1+\left(\frac{z}{z_0}\right)^2\right], \quad R(z) = z\left[1+\left(\frac{z_0}{z}\right)^2\right], \quad (2)$$

where z_0 is defined as the z location where the $1/e^2$ radius has expanded to $\sqrt{2}w_0$. When there is a series of physical objects through which an incident beam passes, the wavefront modification is obtained by simply multiplying the amplitude and phase modulation caused by each independent object. We characterize the modulated field on the image plane by considering the transmission of the agar plate, the colony core, and an edge region. Applying the Huygens-Fresnel principle in rectangular coordinates, this can be expressed as:

$$E_2(x_i,y_i) = \frac{1}{i\lambda}\int\int_\Sigma t(x_a,y_a)E_1(x_a,y_a)\exp\{ik[\phi(x_a,y_a)]\} \times\exp\left(\frac{ikr_{ai}}{r_{ai}}\right)\cos\theta\,dx_a dy_a, \quad (3)$$

where x_i, y_i are points on the image plane, Σ denotes the colony surface, $t(x_a,y_a)$ is the 2-D transmission coefficient, $\phi(x_a,y_a)$ is the 2-D phase modulation factor, r_{ai} is the distance from aperture plane to image plane, and λ is the wavelength. As shown in Fig. 2, R is the radius of the curvature of the bacteria colony, w_b is the $1/e^2$ beam radius, and n_2, Δ_2 and n_3, Δ_3 are the refractive index and thickness of the BHI agar and the Petri dish, respectively. Based on the diffraction theory, assuming its validity criteria[14] are met, the diffracted field on the image coordinates can be approximated as:

$$E_2(x_i,y_i) \approx C_1\int\int_\Sigma t(x_a,y_a)\exp\left[-\frac{(x_a^2+y_a^2)}{w^2(z_1)}\right] \times\exp[ik\phi'(x_a,y_a)] \times\exp[-i2\pi(f_x x_a+f_y y_a)]\,dx_a\,dy_a,$$

$$C_1 = \left\{E_0\exp[ikn_2\Delta_2]\exp[ikn_3\Delta_3]\exp[ik(z_1+z_2)] \times\exp\left[\frac{ik}{2z_2}(x_i^2+y_i^2)\right]\right\}\Big/ i\lambda z_2, \quad (4)$$

where C_1 is the constant outside of the integrals, f_x and f_y are defined as $x_i/\lambda z_2$ and $y_i/\lambda z_2$, $\phi'(x_a,y_a)$ is the total phase modulation, which is contributed from the shape (quadratic phase) and internal structure of the colony, assuming that the convex shape of the colony is assumed and expressed as a phase modulation. More detailed derivation of the model and explanation of the parameter is published in an other paper.[12]

3 Experimental Results

3.1 *Forward Scatterograms*

Figure 1 provides the definition of the parameters used in the experiment. L is the distance between bacterial colonies and the imaging plane, d is the bacterial colony diameter, $\theta/2$ is the maximum half scattering angle of the edge of the scattering pattern, and X_{out} and X_{in} are the linear dimensions of the outer most and brighter inner ring pattern. L is set to 300 mm and 40 mm for the forward scatterometer and BARDOT. Fig-

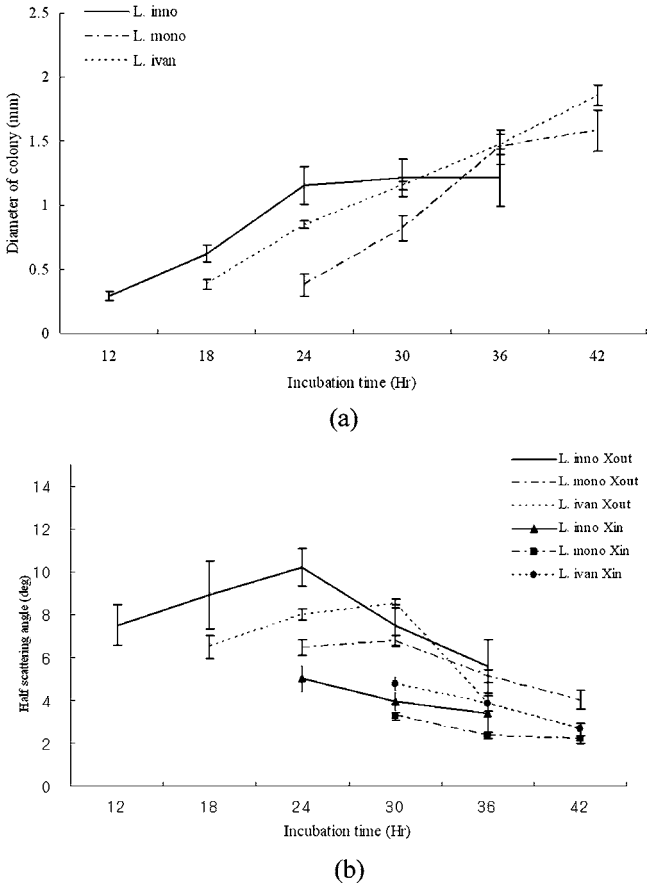

Fig. 3 Result of time-dependent scattering measurement for three types of *Listeria* species: *Listeria innocua, L. ivanovii,* and *L. monocytogenes*: (a) incubation time versus colony diameter; (b) incubation time versus scatterogram diameter.

ure 1 also shows the sample image from the measurement. The top image is from the forward scatterometer, and the bottom is from the BARDOT system for *Listeria innocua* incubated 36 h at 37 °C. A $1/e^2$ beam diameter is selected to match the size of the colony diameter in the stationary phase of the sigmoid growth curve. When the laser beam is smaller than the bacterial colony, the colony outside of the incident beam does not contribute to the scattering signal even though there exist amplitude/phase modulators. Both images show multiple concentric rings, along with a brighter ring in the middle. The BARDOT image shows the pattern in detail from the same colony with higher resolution.

The result of the time-dependent measurement is summarized in Fig. 3. Figure 3(a) shows the relationship between the incubation time and the average diameter of the bacterial colony. The three different species showed different rates of growth. *Listeria innocua* was distinguishable to the human eye and reached a diameter of approximately 0.3 mm. This species showed scattering patterns as early as 12 h and reached the stationary phase after about 24 h. *Listeria monocytogenes*, which grew slower than *Listeria innocua*, started to show scattering patterns around 24 h and reached the stationary phase around 36 h. *Listeria ivanovii* forward scattering was visible around 18 h, and their stationary phase was reached after 42 h. Statistical results of the measurement are summarized in Table 1 with the mean and standard deviation of bacterial colony diameter and maximum half scattering angle.

Figure 3(b) shows the relationship of incubation time versus linear dimension of the scatterogram. We can see that for all three *Listeria* species: (1) there is a growth time and colony diameter that creates the maximum scattering angle, and (2) the inner bright ring starts to appear after a certain incubation time. The maximum outer diameter increases and hits a peak value at 30 h for *Listeria innocua* and at 36 h for *Listeria ivanovii* and *Listeria monocytogenes*. After that, the dimension of the scatterogram tends to decrease with its half scattering angle of 4 to 5 deg. The inner bright rings appear after 24 h for *Listeria innocua* and 30 h for *Listeria ivanovii* and *Listeria monocytogenes*. Therefore, considering both the time and the differentiability, a map of incubation time versus the scattering pattern could be summarized for the three *Listeria* species, as shown in Fig. 4. The top, middle, and bottom rows show the scatterogram variations for *Listeria innocua*, *Listeria monocytogenes*, and *Listeria ivanovii*. This map provides an overall picture of the dependence of scatterogram properties versus growth time, which can provide the characteristic pattern for individual bacterial species or provide the experimental protocol for incubation time. To provide minimal variation in the scatterogram for the current instrument setup, we use an incubation time for which the specific species are in the stationary phase, which is 30 h for *Listeria innocua* and *Listeria ivanovii* and 36 h for *Listeria monocytogenes*.

3.2 *Phase Contrast Microscope*

According to Fig. 4, scatterograms show distinctive patterns for different species. For example, a 30-h grown *Listeria ivanovii* colony shows a speckle effect around the center of the scatterogram, while *Listeria monocytogenes* displays radial spoke features. Although these features are possible candidates for automated image analysis, the biophysical characteristics that cause the distinctive scattering patterns are of most interest here. Figure 5(a) shows the phase contrast microscope image taken for *Listeria ivanovii* at 36 h. This image provides the measured diameter of the bacterial colony and information about the mechanism of formation of the speckle cells, which are circular features 50 to 100 μm in diameter. These circular speckle features are not observed in early hours of incubation but started to appear in the 30-h samples. Figure 5(b) shows the same result for *Listeria monocytogenes* for 36 h of incubation. This species also shows circumferential or arc-shaped features that are not observed in any other species.

4 Discussion

The time-dependent scattering experiment produced valuable results that could provide the origin of the difference of the scattering along with the degree of variation of the scatterogram. The two characteristics observed from Fig. 4 can be explained as follows. We postulate that the first effect is caused by the relationship between fixed laser spot size, the varying colony diameter, and the spatial variations of the density of the bacteria and of the intercellular material excreted

Table 1 Statistical parameters for the time-dependent measurement of three *Listeria* species.

Time (h)	Parameter	*L. innocua*		*L. ivanovii*		*L. monocytogenes*	
		$\theta/2$ (deg)	d (mm)	$\theta/2$ (deg)	d (mm)	$\theta/2$ (deg)	d (mm)
12	μ	7.44	0.29	-	-	-	-
	σ	0.92	0.03	-	-	-	-
18	μ	8.83	0.62	6.48	0.39	-	-
	σ	1.54	0.06	0.51	0.04	-	-
24	μ	10.1	1.15	7.99	0.85	6.44	0.38
	σ	0.86	0.15	0.28	0.032	0.35	0.086
30	μ	7.44	1.22	8.49	1.16	6.77	0.82
	σ	0.94	0.14	0.19	0.035	0.26	0.10
36	μ	5.55	1.38	3.86	1.48	5.13	1.45
	σ	1.21	0.22	0.36	0.08	0.31	0.13
42	μ	-	-	2.64	1.85	4.02	1.58
	σ	-	-	0.28	0.084	0.43	0.16

μ, σ are the mean and standard deviations of 15 samples/plate.

during the growth process. When the colony diameter exceeds the laser spot diameter, additional growth of the outer colony has no effect on scattering pattern. However, we observe a decrease in the scattering pattern diameter, which suggests that some physical aspects of the colony continue to change. But in the stationary phases, the size of the scattering pattern varies, while the scattering pattern itself stays relatively similar compared to the exponential phase where the colony is growing rapidly. The second observation is explained similarly. X_{in} starts to appear after a certain growth time, which suggests some variation in the optical properties of the colony creating the bright ring. One possible explanation is that as bacteria are accumulated in the central core of the colony, the

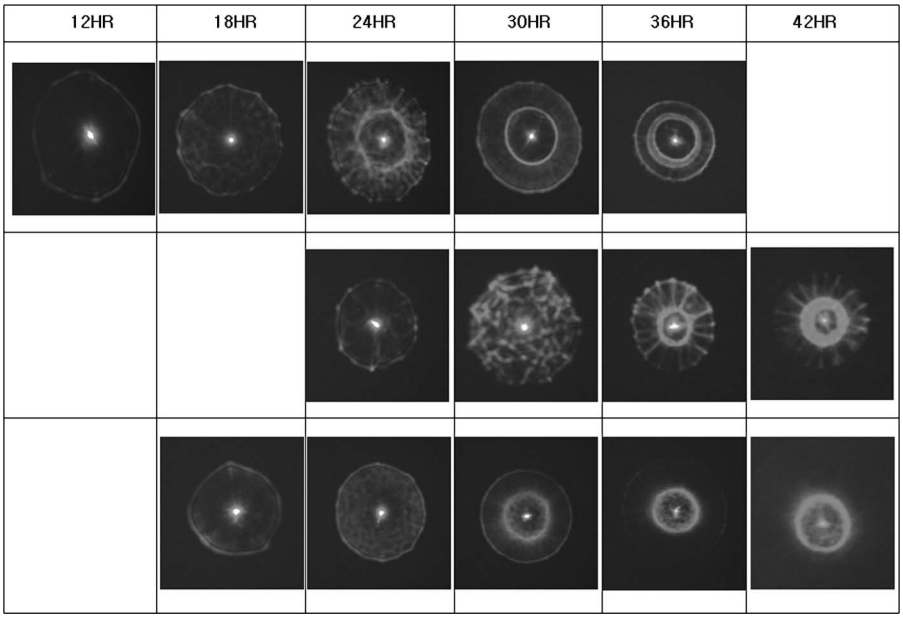

Fig. 4 Incubation time versus scattering pattern of three *Listeria* species: top row—*Listeria innocua;* middle row—*Listeria monocytogenes,* bottom row—*Listeria ivanovii.*

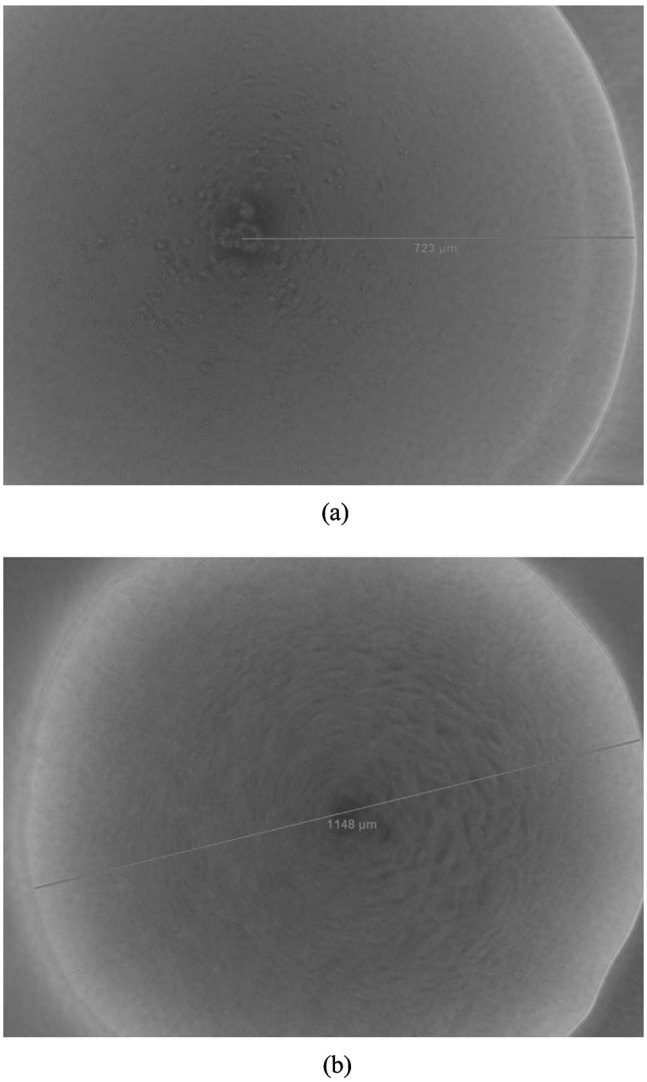

Fig. 5 Comparison of phase-contrast microscope image, which shows unique features: (a) *Listeria ivanovii,* 36 h; (b) *Listeria monocytogenes,* 36 h.

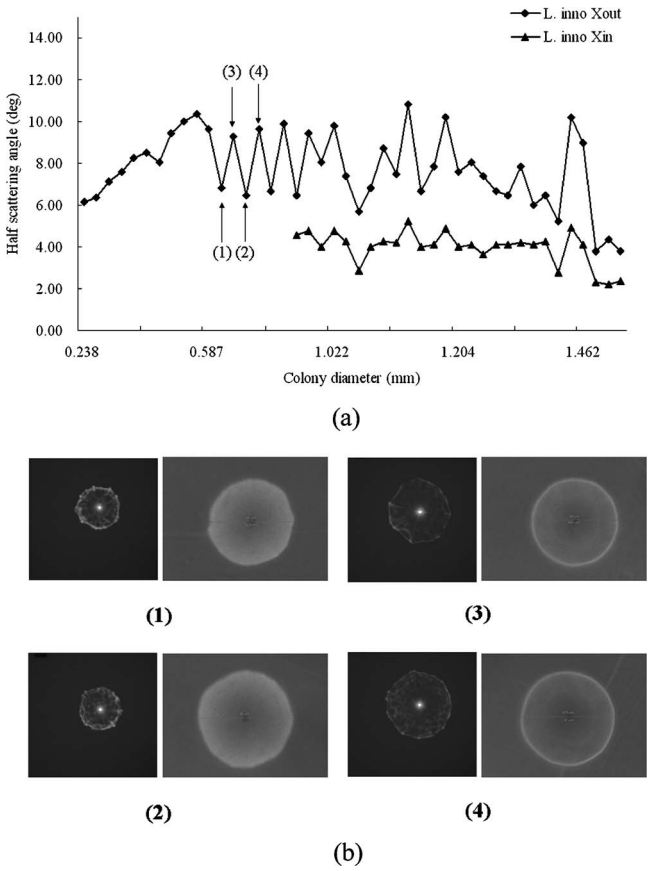

Fig. 6 Scattering pattern and phase-contrast microscope image for *Listeria innocua* that are grown 18 h: (a) colony diameter versus scatterogram diameter; (b) four samples of colony scatterogram and corresponding phase-contrast microscope image.

transmission of the incident light will decrease. The bacteria in the center are possibly dead or dying and attenuate the light (through scattering or absorption), thereby reducing the amount of light transmitted through the center, i.e., a "hole" is created in the center part of the transmitted laser beam. This phenomenon is similar to blocking the center part of a circular laser beam with a stop, which creates a circularly symmetric knife edge pattern along the circumference.[22]

Close investigation of the variation of the scatterograms in Fig. 4 shows similar characteristics between *Listeria innocua* at 24 h and *Listeria monocytogenes* at 36 and 42 h. First, these two figures are clearly similar to the human observer and suggest that a quantitative method to discriminate and classify the scatterogram would be feasible. Second, the radial spoke features in *Listeria innocua* scattering patterns occur during the log phase and disappear after 30 h of incubation, while *Listeria monocytogenes* is in the stationary phase on the growth curve and appears until 42 h of incubation. This result provides a rationale for including an additional time parameter in the discrimination and classification process that will increase the differentiability among species. Another interesting point is that *Listeria ivanovii* is the least transmissive of the three species. At 36 and 42 h, *Listeria ivanovii* X_{out} starts to disappear, while for the other two species it remains visible.

To explain in more detail, we have sorted the data in Fig. 3(b) for each species such that the relationship of bacterial colony diameter and maximum half scattering angle is revealed. Fig. 6(a) shows the sorted data ascending by bacterial colony diameter. Three different growth regions are shown. The first region is up to colony diameter of 585 μm, where the scatterogram diameter is proportional to bacterial colony diameter. When incident light is passed through the aperture, angular distribution of the pattern is inversely proportional to the diameter of the aperture. However, the bacterial colony is more close to a circular stop, since the agar shows 90% transmission with no phase modulation while the bacterial colony shows radial amplitude and phase modulation from Eq. (4). A similar effect is observed in the analysis of the SPM of the nematic liquid crystal film.[19–21] Given a constant film thickness of the liquid crystal film, the result indicates that interference is generated by the phase difference caused by the difference in spatial intensity of the Gaussian incident beam that modulates the nonlinear phase relationship. When the modulated wavefront shows the same gradient from a differ-

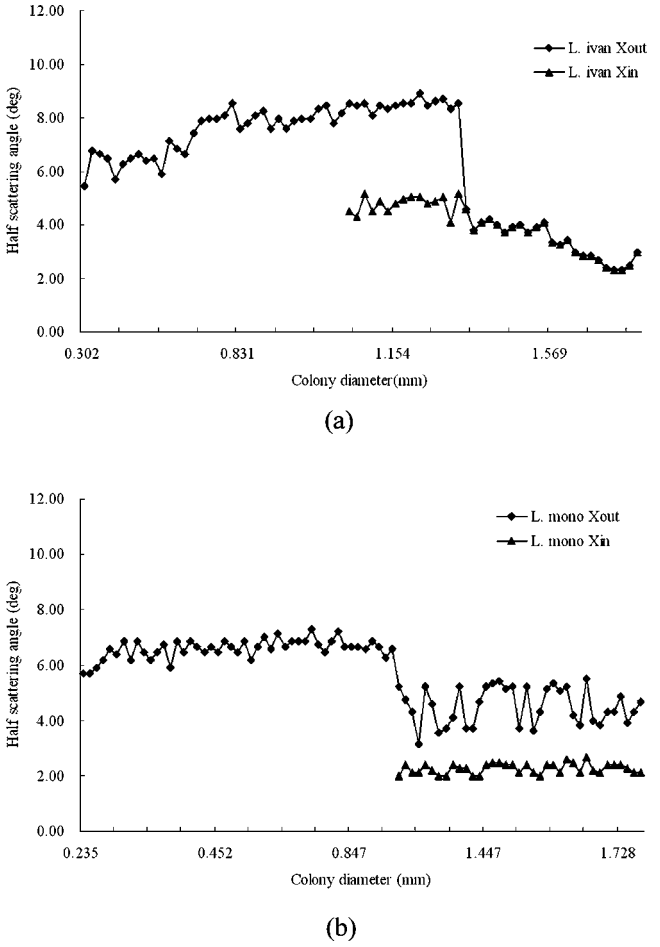

Fig. 7 Colony diameter versus half-scattering angle of scatterogram: (a) *Listeria ivanovii*; (b) *Listeria monocytogenes*.

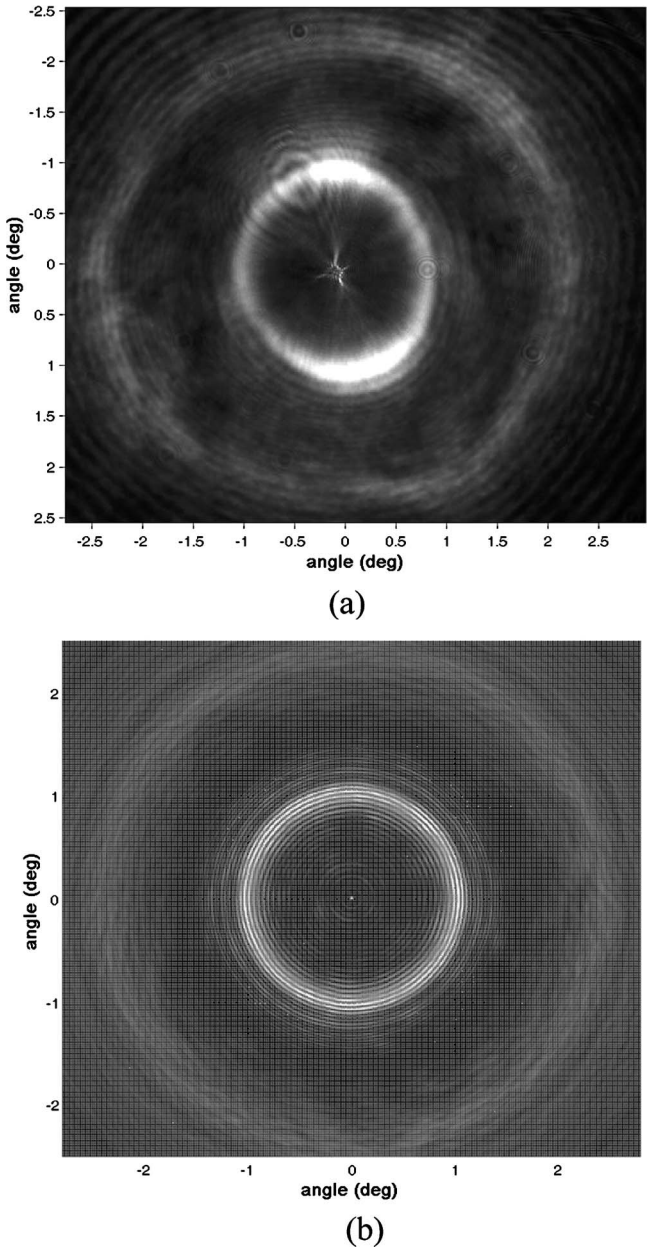

Fig. 8 Comparison of BARDOT image and computational model of *Listeria ivanovii* at 30 h of incubation with a distance of 40 mm: (a) BARDOT; (b) model.

ent spatial location, the scattered light has same wave vector and creates an interference pattern at the far-field. The maximum scattering angle is determined by the maximum absolute value of the gradient of the wavefront right after the light passes the film. While the liquid crystal film has constant film thickness with different phase modulation, the bacterial colony has a dome-shaped colony profile that can produce the same effect because the phase modulation is the multiplication of path length and refractive index.

The second region is up to colony diameter of 1.25 mm, where there is some random variation in scatterogram sizes. To explain this, we have selected four data points and closely observed the phase contrast images. Figure 6(b) shows the scatterogram and corresponding phase contrast microscope image for *Listeria innocua* at 18 h. The image pair numbered (1) and (2) showed 6.84 and 6.47 deg, while (3) and (4) showed 9.28 and 9.65 deg of maximum half scattering angles. Even though the colony diameter is similar, the difference in modulation and the gradient of the wavefront can change the maximum scattering angle, which may be caused by the variation in refractive index, thickness, or volume concentration, etc. The third region is where colony diameter exceeds 1.25 mm, which is closely related to the fixed incident beam diameter. The current experiment employs a 0.635-μm diode laser with 1-mm $(1/e^2)$ diameter. Therefore, additional growth of the bacterial colony that exceeds this region will not be sensed by the incident photons, and other macroscopic parameters such as curvature can affect the extent of the scatterogram. Similar results are found for *Listeria ivanovii* and *Listeria monocytogenes*, as shown in Fig. 7. We applied the previous equation with its individual amplitude and phase modulation terms, as shown in Fig. 8. The amplitude modulation is modeled as the multiplication of the transmission coefficient and the Gaussian beam profile, while the phase modulation is modeled in terms of a convex surface profile.[13,14] The left figure shows the $z=40$ mm scattering pattern from *Listeria ivanovii* at 30 h. The BARDOT system

revealed more detail in the scatteringpattern compared to forward scatterometer images. For example, Fig. 8(a) shows another bright ring at the center. According to the physical model of Eq. (1), the innermost bright ring, which measures about 1 deg, originated from the nondeviated portion of the incident beam, which is incident on the bare agar area. The brighter ring, which measures about 2.5 deg, is the dimension of the X_{in}, which starts to appear after 30 h. As shown in Fig. 8(b), the random speckle effect originates from a circular phase object that we modeled with 50 circles of 20 to 40 μm diameter. The phase value was randomly set between $-\pi$ to π.

5 Conclusion

Time-resolved forward-scattering experiments were performed on colonies of three species of bacteria: *Listeria innocua*, *Listeria monocytogenes*, and *Listeria ivanovii*. The samples were incubated up to 42 h on BHI agar, and two scattering patterns and a phase contrast microscope image were recorded. The scattering patterns varied as a function of growth time, and were related to the fixed beam diameter, bacterial colony diameter, and the spatial distribution of optical amplitude and phase properties across the colonies. The phase contrast microscope images showed distinctive features for different species that were also incorporated in the modeling of the scattering response from the colony. A relationship of scatterogram variation versus growth time was discovered and reported here, which provides the overall picture of scatterogram variation against the growth phase of the bacterial colony. The results and resulting understanding of the relevant biophysical processes provided the basis for a laboratory protocol for the scattering experiments and for differentiating *Listeria* species.

Acknowledgments

This research was supported through a cooperative agreement with the Agricultural Research Service of the US Department of Agriculture Project No. 1935-42000-035 and the Center for Food Safety and Engineering at Purdue University.

References

1. G. D. Curtis, R. G. Mitchell, A. F. King, and E. J. Griffin, "A selective medium for the isolation of Listeria monocytogenes," *Lett. Appl. Microbiol.* **8**, 85–98 (1989).
2. A. D. Hitchins, in *Food and Drug Administration Bacteriological Analytical Manual*, 8th ed., AOAC International, Gaitherburg, MD (1998).
3. R. Schmehl, B. M. Nebeker, and E. D. Hirleman, "The coupled-dipole method for scattering by particles on surfaces using a two-dimensional fast Fourier transform technique," *J. Opt. Soc. Am. A* **14**, 3026–3036 (1997).
4. P. J. Wyatt, "Differential light scattering: a physical method for identifying living bacterial cells," *Appl. Opt.* **7**(10), 1879–1896 (1968).
5. J. D. Andrade, R. A. Vanwagenen, D. E. Gregonis, K. Newby, and J. N. Lin, "Remote fiber-optics biosensors based on evanescent-exited fluoro-immunoassay: concept and progress," *IEEE Trans. Electron Devices* **32**(7), 1175–1179 (1985).
6. Y. L. Pan, S. Holler, R. K. Chang, S. C. Hill, R. G. Pinnick, S. Niles, J. R. Bottiger, and B. V. Bronk, "Real-time detection and characterization of individual flowing airborne biological particles: fluorescence spectra and elastic scattering measurements," *Proc. SPIE* **3855**, 117–125 (1999).
7. P. H. Kaye, E. Hirst, J. M. Clark, and F. Micheli, "Airborne particle shape and size classification from spatial scattering profiles," *J. Aerosol Sci.* **23**(6), 597–611 (1992).
8. S. Holler, Y. Pan, J. R. Bottiger, S. C. Hill, D. B. Hillis, and R. K. Chang, "Two-dimensional angular scattering measurements of single airborne micro-particles," *Proc. SPIE* **3533**, 64–72 (1998).
9. B. Bronk, S. D. Druger, J. Crégé, and W. P. Van De Merwe, "Measuring diameters of rod-shaped bacteria *in vivo* with polarized light scattering," *Biophys. J.* **69**, 1170–1177 (1995).
10. S. Guo, "Optical scattering for bacteria colony detection and characterization, M.S. Thesis, School of Mechanical Engineering, Purdue University, West Lafayette, IN (2004).
11. P. P. Banada, S. Guo, B. Bayraktar, E. Bae, B. Rajwa, J. P. Robinson, E. D. Hirleman, and A. K. Bhunia, "Optical forward scattering for colony identification and differentiation of *Listeria* species," *Biosens. Bioelectron.* **22**, 1664–1671 (2007).
12. B. Bayraktar, P. P. Banada, E. D. Hirleman, A. K. Bhunia, and J. P. Robinson, "Feature extraction from light-scatter patterns of *Listeria* colonies for identification and classification," *J. Biomed. Opt.* **11**, 034006 (2006).
13. E. Bae, P. P. Banada, K. Huff, A. K. Bhunia, J. P. Robinson, and E. D. Hirleman, "Biophysical modeling of forward scattering from bacterial colonies using scalar diffraction theory," *Appl. Opt.* **40**, 3639–3648 (2007).
14. J. W. Goodman, *Introduction to Fourier Optics*, 2nd ed., McGraw-Hill, Boston (1996).
15. J. T. Verdeyen, *Laser Electronics*, Prentice Hall, Englewood Cliffs, NJ (1995).
16. C. S. Guo, X. Liu, J. L. He, and H. T. Wang, "Optimal annulus structure of optical vortices," *Opt. Express* **12**, 4625–4634 (2004).
17. M. A. A. Neil and E. G. S. Paige, "Improved transmission in a two-level, phase-only, spatial light modulator," *Electron. Lett.* **30**, 445–446 (1994).
18. H. R. Suiter, *Star Testing Astronomical Telescopes*, Willmann-Bell (2003).
19. S. D. Durbin, S. M. Arakelian, and Y. R. Shen, "Laser-induced diffraction rings from a nematic-liquid-crystal film," *Opt. Lett.* **6**, 411–413 (1981).
20. I. C. Khoo, J. Y. Hou, T. H. Liu, P. Y. Yan, R. R. Michael, and G. M. Finn, "Transverse self-phase modulation and bistability in the transmission of a laser beam through a nonlinear thin film," *J. Opt. Soc. Am. B* **4**, 886–891 (1987).
21. K. Ogusu, Y. Kothani, and H. Shao, "Laser-induced diffraction rings from an absorbing solution," *Opt. Rev.* **3**, 232–234 (1996).
22. E. Hecht, *Optics*, 4th ed. Addison-Wesley, Boston (2002).